Appendix A

Mechanically Tunable Thin Films of Photosensitive Artificial Proteins: Preparation and Characterization by Nanoindentation

It should be noted that what follows has been previously published by the authors in *Macromolecules* **2008**, *41*, 1839-1845.

Mechanically Tunable Thin Films of Photosensitive Artificial Proteins: Preparation and Characterization by Nanoindentation

Paul J. Nowatzki[1], Christian Franck[3], Stacey Maskarinec[1], Guruswami Ravichandran[3], and David A. Tirrell[1,2*] (1) Division of Chemistry and Chemical Engineering

(2) Joseph J. Jacobs Institute for Molecular Engineering for Medicine

(3) Division of Engineering and Applied Science

California Institute of Technology, Pasadena, California 91125, USA

Corresponding Author: tirrell@caltech.edu

Abstract

Thin films of controlled elastic modulus were made by photocrosslinking artificial extracellular matrix (aECM) proteins containing the photosensitive amino acid para-azidophenylalanine (pN$_3$Phe). The elastic moduli of the films were calculated from nanoindentation data collected by atomic force microscopy (AFM) using a thin-film Hertz model. The modulus was shown to be tunable in the range 0.3-1.0 MPa either by controlling the irradiation time or by varying the level of pN$_3$Phe in the protein. Tensile measurements on bulk films of the same proteins and finite-element simulation of the indentation process agreed with the thin-film modulus measurements from AFM. Substrates characterized by spatial variation in elastic modulus were created by local control of the irradiation time.

Introduction

Cellular interactions with the surrounding matrix play defining roles in biological processes ranging from normal tissue function to morphogenesis, immunity, wound healing, and tumor metastasis. The realization that substrate mechanical properties strongly influence cell behavior is comparatively recent and has stimulated considerable interest.[1] Substrate stiffness has been shown to affect cell adhesion,[2,3] morphology,[2,4,5] traction forces and migration rate,[2,6,7] growth,[8] and differentiation.[3,9−11].

Cell culture substrates with adjustable mechanical properties have become essential tools for the study of cell-matrix interactions. The stiffness-dependent cell behavior reported to date has been examined most frequently on synthetic gels such as polyacrylamide.[2,6,12] Because biological and mechanical signals are often interdependent,[1,13] some investigators have chosen substrates (e.g., collagen-coated gels) that mimic more closely the natural extracellular matrix.[3,8] Additional advantages accrue from varying mechanical properties on a single substrate, in that many sets of culture conditions can be probed at once, reducing the experimental variability that arises from lot-to-lot variation in the behavior of cultured cells. Moreover, films of spatially varying elastic modulus allow

the examination of cell behavior at mechanical interfaces,6 and elastic modulus gradients allow the study of mechanotaxis or durotaxis.[7,14,15]

Here we describe the use of photosensitive artificial proteins to make substrates on which the interrelated effects of elastic modulus and extracellular matrix biology can be studied directly. These proteins are intended for use as implantable biomaterials, and are designed to mimic key features of the extracellular matrix.[16−19] The design (Figure A.1) includes cell-binding domains periodically spaced between elastin-like repeating elements. The CS5 cell-binding domain, derived from human fibronectin, enables attachment of cells that express the $\alpha_4\beta_1$ integrin adhesion receptor.[20] The origin of the elasticity of the protein is the repeating pentapeptide VPGVG (Val-Pro-Gly-Val-Gly), derived from mammalian elastin and shown by Urry and others to confer mechanical properties appropriate for soft tissue engineering and regenerative medicine.[21]

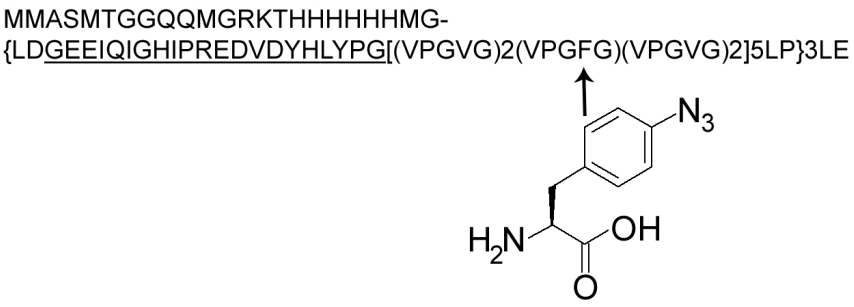

Figure A.1: Amino acid sequence of the artificial extracellular matrix protein examined in this work. The cell-binding sequence CS5 is underlined. Proteins containing the photosensitive amino acid para-azidophenylalanine are designated aE-pN$_3$Phe.

The phenylalanine (Phe) sites encoded within the elastin-like domains of the protein serve as sites for incorporation of the non-canonical amino acid para-azidophenylalanine (pN$_3$Phe, Figure A.1). Incorporation of pN$_3$Phe into recombinant proteins is accomplished by using a bacterial expression host that harbors a mutant phenylalanyl-tRNA synthetase (PheRS) with an enlarged binding pocket.[22,23] Upon photolysis, pN$_3$Phe generates a reactive nitrene intermediate that yields non-specific crosslinks to surrounding protein molecules. Varying the concentration of pN$_3$Phe in the expression medium controls the extent of incorporation of the photosensitive amino acid into the protein, and ultimately determines the crosslink density and elastic modulus of the irradiated

protein film. We recently reported photochemical patterning of similar proteins (and adherent cells) on solid substrates.[24] Here we describe detailed mechanical characterization of thin photocrosslinked protein films and demonstrate the preparation of step-gradients of mechanical properties within a single film.

Mechanical properties of thin, substrate-bound films are typically measured by nanoindentation, and atomic force microscopy (AFM)-based nanoindentation in particular offers significant advantages in spatial and force resolution over conventional nanoindenters. The method is especially attractive for analyzing soft samples and materials whose elastic modulus varies over short length scales.[25−27]

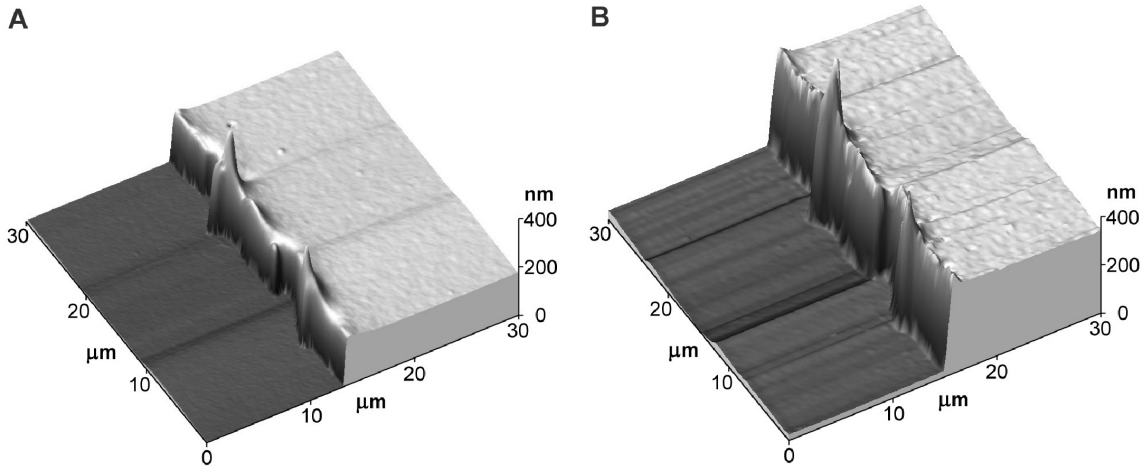

Figure A.2: AFM topography scans of cut edges of an aE-48%-pN$_3$Phe film, dry (A) and in water (B). The spikes at the edge are artifacts of the scratching procedure.

Here AFM nanoindentation with a microspherical tip (600 nm diameter) was used to obtain accurate measurements of the elastic moduli of thin photocrosslinked protein films.[11,28,29] The use of a spherical tip is important, in that it allows a spherical indentation model to be correctly applied; the classical Hertz spherical model is known to cause distortions when used to analyze AFM data collected with conventional sharp, pyramidal or conical tips.[30] A film-height dependent physical model [31] accounts for the mechanical coupling of the film to its underlying substrate, another known source of distortion in AFM nanoindentation.[32,33] Bulk tensile tests of the same materials confirm the validity of the nanoindentation analysis.Finite element simulations of the indentations were also performed to verify the modulus calculations and to explore the possibility of determining a more

sophisticated mechanical material model from the AFM data. While the linear elasticity model [31] accurately characterizes the Young's (elastic) moduli of the films described herein, the finite element analysis is appropriate for characterization of thinner films undergoing large deformations due to higher-strain indentation or certain tip geometries.

Experimental Section

Protein aE-pN$_3$Phe. The amino acid sequence of the photosensitive artificial extracellular protein, aE-pN$_3$Phe, is shown in Figure A.1. aE-pN$_3$Phe is made biosynthetically in a Phe-auxotrophic strain of Escherichia coli outfitted with a plasmid bearing genes coding for both the protein and the Ala294Gly mutant of the *E.* coli phenylalanyl-tRNA synthetase (PheRS).[34] Use of the mutant synthetase allows incorporation of pN$_3$Phe (Bachem) into recombinant proteins in place of Phe.[23] Because the relative amounts of Phe and pN$_3$Phe in the protein can be controlled by varying the concentrations of the amino acids in the expression medium, the designation aE-pN$_3$Phe refers to a family of artificial proteins rather than to a single protein.

The expression and purification of aE-pN$_3$Phe were performed as described previously.[24] To deplete Phe from the expression medium, cells were centrifuged and resuspended in minimal medium lacking Phe and containing pN$_3$Phe 10 minutes after expression was induced. This procedure allows enough time for functional copies of PheRS to be synthesized before Phe is depleted.

The extent of replacement of Phe by pN$_3$Phe was measured by 600 MHz 1H NMR spectroscopy (Varian) at a protein concentration of 15 mg/mL in DMSO-d6 (Cambridge Isotope Laboratories).[24] Phe replacement levels of 28%, 31%, 48%, and 66% were achieved by using 125, 188, 250, and 250 mg/L, respectively, of pN$_3$Phe in the culture medium; the corresponding proteins are designated aE-28%-pN$_3$Phe, etc.

AFM - instrument. Images and force curves were collected on a Park Scientific Instruments AutoProbe M5 atomic force microscope, with accompanying ProScan v1.51b software. Pyramidal-tipped triangular silicon nitride cantilevers with nominal spring constant 0.58 N/m were used for imaging (Veeco DNP-S). A silicon nitride cantilever of the same shape, with an attached 600 nm

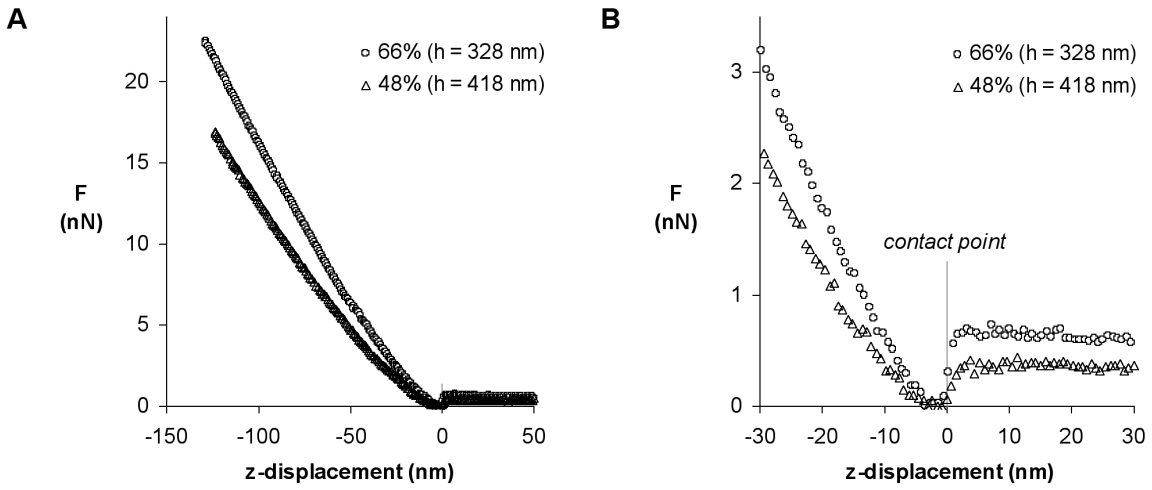

Figure A.3: Representative loading indentation profiles for thin films of aE-66%-pN$_3$Phe and aE-48%-pN$_3$Phe, showing force versus indentation depth (z-displacement). (A) shows the entire profiles; (B) is magnified to show the contact point assignment.

diameter SiO_2 particle tip (Novascan, Ames, IA), was used to indent samples for collecting force curves. The spring constant of the cantilever was calculated to be 0.37 N/m by indenting against reference cantilevers with predetermined spring constants of 1.00 N/m and 0.125 N/m (Veeco CLFC). Here, $k_{test}/k_{ref} = (\delta_{tot} - \delta_{test})/(\delta_{test} cos(\theta))$, where k_{test} and k_{ref} are the spring constants of the test and reference cantilevers, δ_{tot} and δ_{test} are slopes of the force-distance curves when the test cantilever is indented against a rigid surface and against the free end of a reference cantilever, respectively, and θ is the angle between the cantilevers (15^o). A glass slide was glued to the back of the cantilever mount so that the cantilever and sample could be submerged in water.

Bulk protein films. aE-pN$_3$Phe (4 mg) was dissolved in dimethylsulfoxide (40 µL, Mallinckrodt). The solution was spread to cover an area ca. 1.5 cm x 1 cm on a poly(methyl methacrylate) surface, and the solvent was evaporated at 50^oC overnight. The resulting films were ca. 20 µm thick (dry). After photocrosslinking (vide infra), uniaxial tension tests were performed at 22^oC on an Instron 5542 Materials Testing System outfitted with a 0.5 N load cell and modified to contain the sample in a water bath. The nominal strain rate was 0.1 per minute;[35] at this rate viscoelastic effects are negligible.

Thin protein films. All film-making procedures were performed in a cold room (4^oC), below the

lower critical solution temperature (LCST)21 of the protein in water. Protein (10 mg) was dissolved in water (100 μL), and the solution was centrifuged (5 min, 16,500g) to remove any aggregates or particles. Protein solution (10 μL) was pipetted onto and spread to cover an unmodified 12 mm glass slide (Hecht-Assistent, Sondheim, Germany). Films were spin-coated (Specialty Coating Systems, Inc. P6204, Indianapolis, IN) at 7,000 rpm for 30 seconds and dried overnight at 4°C. Typical film thickness was ca. 160 nm (dry).

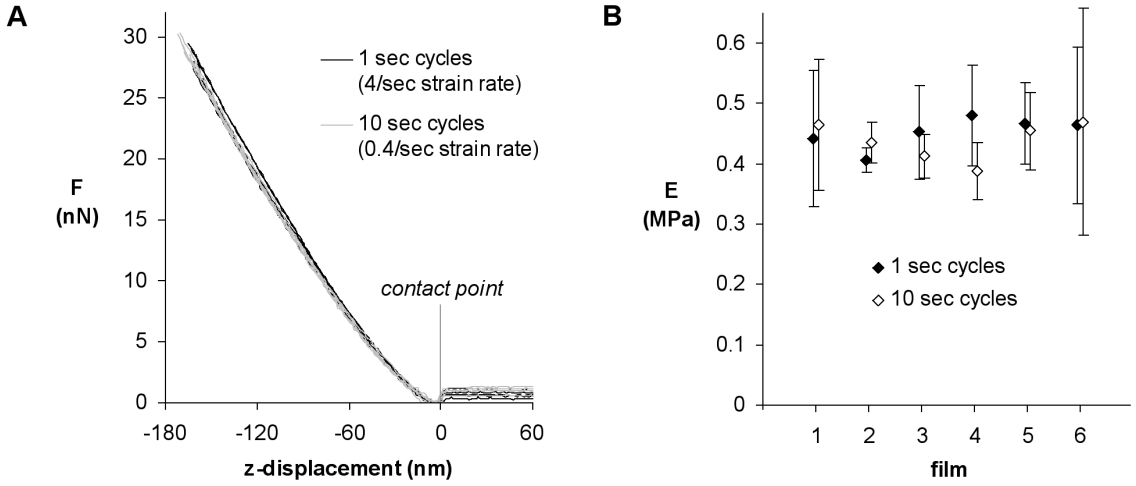

Figure A.4: (A) Superimposed force profiles for multiple indentations of a single aE-48%-*p*N_3Phe film for 1 sec and 10 sec indent cycles. (B) Calculated Young's modulus for 1 sec and 10 sec indentation cycles on five different aE-48%-*p*N_3Phe films.

Irradiation of films. Dry protein films were exposed to unfiltered UV light from a high-pressure mercury arc lamp (Oriel Q, 100 watt @ 5 amps, > 20 min warm-up time; measured intensity in irradiation plane = 1.5 mW/mm2). The time required to achieve complete conversion, ca. 300 sec, was determined empirically. Zones of differential crosslinking were prepared on the same substrate by placing an opaque shutter over portions of the film during irradiation. Specifically, a step-gradient of irradiation times (0, 12, 20, 30, 50, 80, 120, 180, and 300 sec) was made across a 12 mm slide by manually repositioning the shutter between exposures.

Slides were agitated in excess water at 4°C to remove any soluble protein. Un-irradiated protein, or protein irradiated for 12 sec or less, was completely removed during this rinsing process as evidenced by AFM imaging. No delamination of irradiated films from their glass substrates was

protein	pN$_3$Phe added to medium (mg/L)	% replacement of Phe by pN$_3$Phe	protein yield (mg protein/liter of culture)
aE-66%-pN$_3$Phe	250	66	66
aE-48%-pN$_3$Phe	250	48	35
aE-31%-pN$_3$Phe	188	31	76
aE-28%-pN$_3$Phe	125	28	66

Table A.1: Expression conditions and protein yields

observed.

AFM film thickness. The tip of a pair of fine forceps was dragged lightly across the surface of the protein film, tearing away the protein along the scratch and revealing the underlying glass substrate. The edge of this scratch was imaged by AFM both dry and under water; the thickness of the film is apparent from the scan (see Figure A.2). The surface revealed by the scratch was confirmed to be glass, based on its smoothness and linear force profile when indented. The protein film thickness was calculated by averaging the height measurements at many (n $\geq$ 16) points on the film, using the revealed glass surface as a baseline.

AFM indentation force curves. The films and cantilever assembly were submerged in water under ambient conditions. The 600-nm SiO_2 microsphere tip was placed above a spot where the film thickness had been measured (identified visually from the optical microscope image using reference markers on the film) to ensure that the thickness at the point of indentation was known. Force curves were collected; the instrument records z (piezo) displacement, and force, which is the product of measured tip deflection and cantilever spring constant.

The indentation range was set to (-150 nm, +1350 nm) relative to the contact point, effectively limiting the force to ca. 20-30 nN and the strain magnitude to less than 20%. The indent-retract cycle time was 1 sec (tip speed 3 μm/sec). Viscoelastic effects did not appear to be a significant factor at this strain rate (ca. 4 sec 1), as evidenced by the statistical superimposability of force curves collected using 1 sec and 10 sec cycles (strain rate ca. 0.4 sec 1) (Figure A.4).

To assess the uniformity of the films, force curves were evaluated repeatedly at the same spot and at nearby spots spaced 10-20 μm apart. For uniformly irradiated pN$_3$Phe films this procedure

was repeated at three distant (> 1 mm apart) spots of known height.

Calculation of Young's (elastic) modulus. The Dimitriadis model [31] for indentation of linearly-elastic soft material films of finite height with a spherical indenter was applied to the loading force data. For a support-bonded film with Poisson's ratio of $\nu = 0.5$ (incompressible, a reasonable estimate for both for rubbery networks and biological materials):

$$F = \frac{16E}{9} R^{1/2} \delta^{3/2} [1 + 1.133\chi + 1.283\chi^2 + 0.769\chi^3 + 0.0975\chi^4]. \tag{A.1}$$

The first term of this series is the classical Hertz indentation model, giving the force F as a function of (Young's) elastic modulus E and indentation depth δ using a rigid sphere of radius R. The additional terms [31] correct for the finite height of the film, where χ is given by:

$$\chi = \sqrt{R\delta}/h, \tag{A.2}$$

where h is the thickness of the film. As the film gets thinner, or as the indentation depth increases, the indenting sphere (AFM tip) experiences a higher force than it would for an infinitely-thick film of the same material, owing to mechanical effects of film confinement to the stiff underlying substrate. The film indentation δ was calculated by subtracting the tip displacement from the total (z) displacement.

The contact point of each force-distance curve, where the indentation and force were set to zero in the analysis, was determined by visual inspection. While this can be difficult in some experiments, [31] it is straightforward for the force curves collected here, because we observe a distinct snap-in when the tip touches the surface (see Figure A.3 for examples). The apparent elastic modulus was calculated by evaluating equations A.1 and A.2 at each recorded force-indentation point between 15 nm and 10% film thickness indentation and averaging over the range. Below 15 nm, the scatter in the data is magnified in the calculations and distortions are common; the 10% maximum indentation constrains the data to the near-linear response range.31 In this strain range, the finite-height correction factor was as large as 1.78 ($\chi = 0.395$) for the films analyzed here.

Finite element simulation. Simulations of the nanoindentation process were conducted by using the commercial finite element software, ABAQUS (ABAQUS, Inc., Providence, RI). The geometries of the indenter and the film were discretized by using 2D axisymmetric elements ($CAX4R$) and the known protein film height and indenting spherical tip geometry ($R = 300$ nm). From tensile data collected for bulk samples of aE-pN$_3$Phe, material model parameters for each material were calculated and entered into the simulation. Various hyperelastic material models describing the large strain material behavior (e.g., Neo-Hookean, Mooney-Rivlin, etc.) were evaluated. The Yeoh model [36] was found to best describe the material response of aE-pN$_3$Phe as determined through numerous uniaxial tension and compression tests. The output of force versus film indentation was compared to the AFM data collected experimentally.

Results And Discussion

Protein production and purification. aE-pN$_3$Phe proteins were expressed in a phenylalanine-auxotrophic $E.$ coli expression host using a medium shift procedure which allowed controlled replacement of phenylalanine by pN$_3$Phe. Cells were grown for several hours in media containing all 20 natural amino acids, washed and transferred to minimal media containing 19 amino acids and lacking phenylalanine. Production of the mutant PheRS during the initial growth period provides the cellular machinery needed for insertion of pN$_3$Phe into recombinant proteins. Target proteins were collected from harvested cells and separated from contaminant proteins through a series of temperature-shift centrifugation cycles24, and protein purity was monitored by denaturing gel electrophoresis. Titrating the amount of pN$_3$Phe in the expression medium generated artificial proteins containing controlled levels of incorporation of the photosensitive amino acid (Table A.1).

Thin films. Spin-coated thin films of aE-pN$_3$Phe proteins appeared smooth (RMS roughness = 1.3 nm, versus 0.9 nm for the revealed glass) when imaged by AFM (Figure A.2). Film thickness was uniform over the surface of each 12 mm diameter glass substrate, varying no more than 11% from the average. Local thickness was much more uniform, with $< 2\%$ variation in a 30 μm scan. The protein films had average hydrated thicknesses between 206 and 368 nm, except for two films

protein	thickness (μm)	average elastic modulus, E (MPa)	molecular weight between crosslinks, Mc	pN$_3$Phe crosslinking reaction efficiency (%)
aE-66%-pN$_3$Phe	20	1.01 ± 0.07	4300 ± 200	50 ± 3
aE-48%-pN$_3$Phe	21	0.52 ± 0.04	7000 ± 400	42 ± 2
aE-31%-pN$_3$Phe	19	0.20 ± 0.04	11,900 ± 1000	39 ± 3
aE-28%-pN$_3$Phe	20	0.14 ± 0.02	13,800 ± 600	37 ± 2

Table A.2: Physical properties of bulk aE-pN$_3$Phe films tested in uniaxial tension (n=2).

protein	average hydrated thickness of each tested film (nm)	average elastic modulus, E (MPa)	molecular weight between crosslinks, Mc	pN$_3$Phe crosslinking reaction efficiency (%)
aE-66%-pN$_3$Phe	312, 322, 328, 1682, 1466	0.91 ± 0.16	4900 ± 700	45 ± 7
aE-48%-pN$_3$Phe	293, 368	0.44 ± 0.04	7800 ± 400	38 ± 2
aE-31%-pN$_3$Phe	223, 252	0.30 ± 0.02	9800 ± 400	47 ± 2
aE-28%-pN$_3$Phe	206, 206	0.29 ± 0.03	10,000 ± 500	51 ± 3

Table A.3: Physical properties of thin aE-pN$_3$Phe films tested by AFM (n6 spots, n24 total indents).

ca. 1500 nm thick, which were made by using a higher concentration of aE-66%-pN$_3$Phe (Table A.3). The average ratio of wet-to-dry film thickness was 1.80, corresponding to a polymer volume fraction of 0.56 in the hydrated films. We observed little variation in the polymer volume fraction under the conditions used here.

AFM Force Curves. Representative loading force-displacement curves are shown in Figure A.3, and exhibit the parabolic shape typical of indentation of soft materials. Since the assembly is submerged in water, the attractive force between the tip and the surface is screened; nevertheless, a distinct snap-in event appears in each force curve, and allows a contact point to be confidently assigned.

In cases where snap-in appeared to occur over a few nanometers, the contact point was assigned to the middle of the snap-in rather than the bottom (at minimum force); this procedure was found to give the best reproducibility between repeated indentations at the same spot. Adhesion forces between the indenter and sample appeared to be negligible during indentation loading, and finite element simulations confirmed this interpretation.

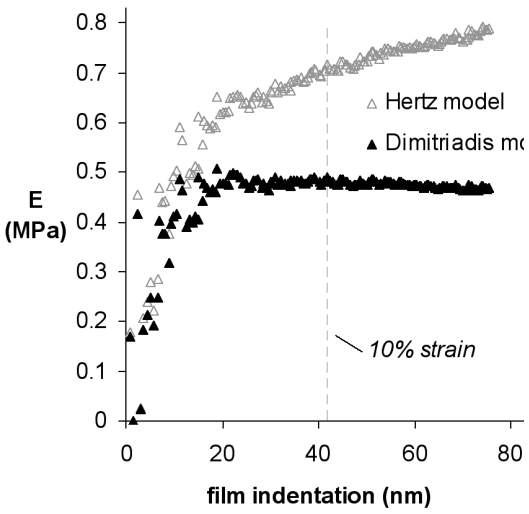

Figure A.5: The elastic modulus (E) calculated at each point in the AFM indentation using Hertz and Dimitriadis models (Eq. A.1) is shown for an aE-48%-pN$_3$Phe film.

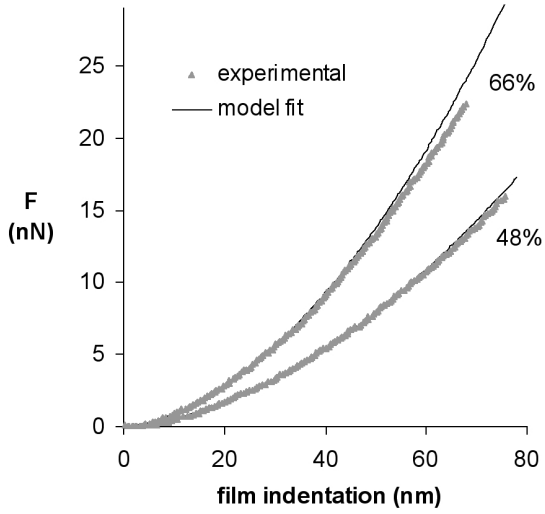

Figure A.6: Experimental AFM indentation data compared to Dimitriadis model (Eq. A.1) fits for thin films of aE-66%-pN$_3$Phe and aE-48%-pN$_3$Phe.

When the strain rate was reduced by a factor of 10 (from a 1 sec indentation cycle, strain rate ca. 4 sec-1), the resulting force curves appeared indistinguishable from the originals, indicating that viscoelastic effects did not significantly influence the results (Figure A.4) in the range of loading rates considered here (0.4 to 4 sec-1). Faster indentation cycles allow increased throughput and minimize the deleterious effects of sensor drift.

Repeated indentations (up to 100) of the same spot did not cause any change in the force-displacement curves, likely because the hydrated protein films are highly elastic (albeit nonlinear) and the indentation depth was controlled. When surfaces on which the indentations had been performed were subsequently imaged by AFM, no evidence of indentation was seen on either hydrated or dry films. These results suggest that the collection of force curves did not permanently deform or otherwise alter the mechanical properties of the samples.

Analysis of AFM force curves. Once a force curve is collected, all variables except E in Eqs. A.1 and A.2 are known, so each point on the force-distance curve can be used to calculate an elastic modulus for the material. If the model describes the system correctly, the calculated modulus should be the same at each indentation depth. The Hertz and Dimitriadis [31] models were evaluated using

this criterion for a representative data set (Figure A.5). Because the films were less than a micron in thickness and the indentation depth represented a significant portion of the film height, the Hertz model for infinite-height film was inappropriate for elastic modulus calculation. The effective elastic properties of the protein films were significantly influenced by the underlying glass substrate, as has been observed previously for soft thin films.[31,32]

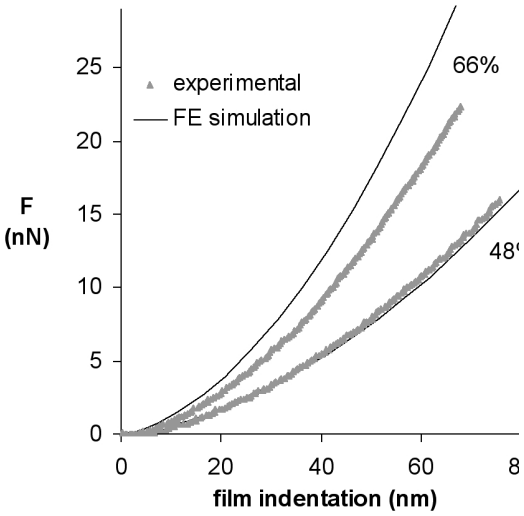

Figure A.7: Superposition of experimental AFM data and finite element simulations of indentation based on bulk tensile data for thin films of aE-66%-pN$_3$Phe and aE-48%-pN$_3$Phe.

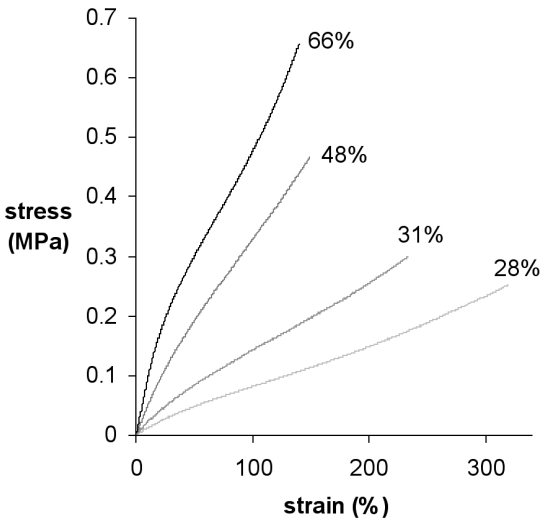

Figure A.8: Sample tensile data for bulk films containing varying amounts of pN$_3$Phe.

Because it accounts for finite sample thickness and coupling to a rigid substrate, the Dimitriadis model is able to extract the true elastic modulus of the protein film, thus yielding much more consistent predictions of thin film modulus for each force curve in the indentation depth range of 15 nm to 10% (or more) of the film thickness.

A single value of Young's modulus (E) was assigned to each surface by averaging the model-predicted moduli from 15 nm to 10% strain; the standard deviation in E over this range averaged 3.4% and was $< 10\%$ for all curves, indicating that the Dimitriadis model gives uniform predictions of E. In general, the model-calculated value of E is sensitive to the placement of the contact point,[31] but since contact is observed directly and the sub-15 nm data (recorded forces < 1 nN) are excluded, the fits are robust. Illustrations of the fit of the Dimitriadis model to the experimental AFM data

are shown in Figure A.6.

The standard deviation in E from repeated indentation of the same spot (n=3-4 indentations, 51 spots) averaged 5.1%. We observed no tendency of the film to change in modulus with repeated indentation. The standard deviation in E between different spots on the same film (n=3-4 spots,$\geq$10 μm apart, 13 films) averaged 7.2%, nearly as small as the same-spot variance, indicating that E was uniform over the films. The uniformity of modulus is important for the application of these films as probes of mechanosensitive cell behavior.

In principle, raw AFM data could be used to estimate film thickness, by iterating the height parameter in Eq. A.2 to minimize the variation in predicted modulus over the selected strain range, since over- or underestimated thickness will result in less consistent modulus predictions. For this technique to be applied, the linear model would need to completely describe the material mechanics in the analyzed strain range. However, experimental error makes it likely that decreases in film thickness could be mistaken for increases in elastic modulus, or vice-versa. The determination of modulus is more accurate when the film thickness is known, as it is here.

Finite element simulation of indentation. All bulk tensile data were well-described by a Yeoh hyperelastic model.[36] When the Yeoh parameters calculated from the tensile data (vide infra; see Figure A.8) were used to model indentation using a finite element simulation, the predicted force-displacement curves were very similar to those obtained experimentally; representative data are presented in Figure A.7. Because of the experimental error in measuring quantities such as the bulk film thickness or AFM cantilever spring constant, some differences in scalar magnitude between these two plots can be expected, although their shapes should be similar, as observed. The similarity between experimental AFM indentation data and simulations of the indentation using only bulk tensile properties is encouraging since it implies that the physical properties of thin and bulk films are similar, and it confirms the validity of the finite element analysis technique.

The samples investigated here are thick relative to the indentation depth and are highly elastic, so the deviations from linearity are small, as can be seen by comparing the linear model fit with experimental AFM data in Figure A.6. However, the simulation approach should be applicable

to thinner films (e.g., <100 nm) and to non-linear strain data as well, where a limited amount of data can be collected in the linear deformation range. While the Dimitriadis model is restricted to spherical tips, the simulation can be easily changed to describe conical or pyramidal tips, the type more commonly used because of their robustness and lower cost. These sharp tips have the additional advantage of being usable for imaging as well as indentation.

In performing the inverse analysis of predicting the AFM response from the tensile data, we used the AFM data to calculate a modulus for the material using the simulation. Coefficients of the Yeoh model were iterated in the finite element simulation to minimize the difference between the simulated and experimental AFM data using the entire force curve (including indentation data past 10% of the film thickness). The moduli determined in this way were indistinguishable from those calculated with the Dimitriadis model. If high-strain data are collected, this technique can provide the complete strain energy function for the material being tested in addition to the elastic Young's modulus (E). While the finite element technique provides more flexibility, the simplicity of the Dimitriadis model is preferable when the geometry of the tip is known and when the linear elastic modulus is the only value required.

Modulus control by variable incorporation of *p*N_3Phe bulk films. As described earlier, the extent of incorporation of $p$$N_3$Phe into a$E$-$p$$N_3$Phe proteins can be controlled by varying the concentration of the photosensitive amino acid in the expression medium. We examined the effects of variable incorporation of $p$$N_3$Phe, both for bulk samples tested in uniaxial tension and for thin-film samples analyzed by AFM nanoindentation.

The tensile behavior of the bulk samples (Figure A.8) is typical of rubbery materials; all aE-$p$$N_3$Phe films were extensible to 150% (or greater) strains. As expected, the modulus increases with the $p$$N_3$Phe content of the protein, a result of increased crosslink density after irradiation. If the materials are assumed to behave as ideal rubber networks, the shear modulus (G) can be related to the crosslink density through the expression[37]:

$$G = (\rho RT/M_c)(1 - 2M_c/M), \tag{A.3}$$

an approximation shown to be valid for similar elastin-like hydrogels.[17,35] The shear modulus is equal to one-third of the elastic modulus for an incompressible material (ν=0.5), a good approximation for rubbery hydrated protein films. The chain mass density ρ is found by multiplying the density of elastin[3]8 (1.32 g/cm^3) by the measured polymer volume fraction (0.56) in the films, M_c is the average molecular weight between crosslinks, and the term (1-2M_c/M) represents the fraction of elastically active crosslinks, where M is the molecular weight of the protein (42,900). The values of M_c calculated for the films examined here are listed in Table A.2.

The efficiency of crosslinking can be calculated from Mc and the pN$_3$Phe content of the protein. For example, the value of Mc (4300) estimated for aE-66%-pN$_3$Phe corresponds to ca. 10 (42,900/4300) crosslinks per protein chain, assuming random crosslinking a reasonable assumption given the periodic Phe spacing in the protein and the statistical nature of its replacement by pN$_3$Phe. Incorporation of the photosensitive amino acid at 66% of the 15 Phe sites yields an average of 9.9 pN$_3$Phe side chains per molecule; because each crosslinking event couples two molecules, the measured value of Mc indicates a reaction efficiency of ca. 50% (10/9.9/2). The crosslinking efficiency declines slightly as the pN$_3$Phe content of the film is reduced (Table A.2).

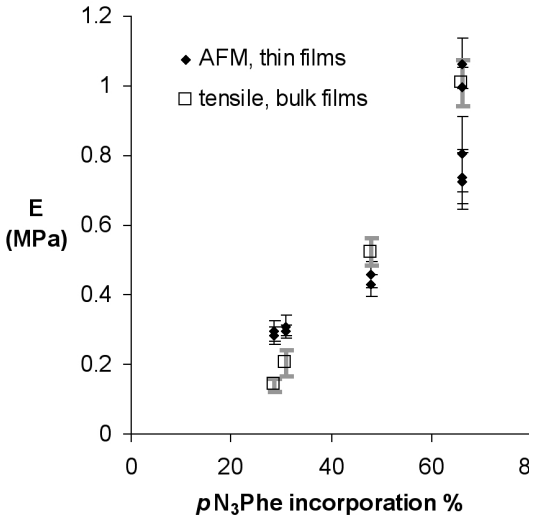

Figure A.9: Measured elastic moduli of thin films of aE-pN$_3$Phe versus fraction replacement of Phe by pN$_3$Phe. Results from AFM nanoindentation of thin films and tensile testing of bulk films are compared.

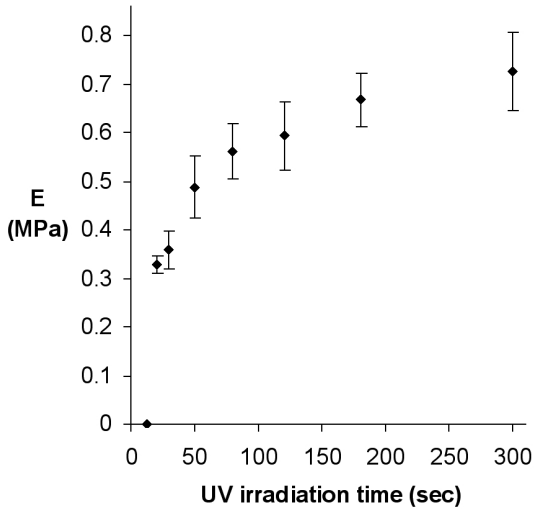

Figure A.10: Preparation of a step gradient in elastic modulus by variable irradiation of a single aE-66%-pN$_3$Phe film. Error bars indicate standard deviation in modulus within each zone of the gradient.

Modulus control by variable incorporation of pN$_3$Phe thin films. Figure A.9 compares the elastic moduli calculated from AFM data for thin films to those measured for bulk films in uniaxial tension. For aE-48%-pN$_3$Phe and aE-66%-pN$_3$Phe, the values match within experimental error, indicating that the mechanical properties of the bulk films can be reproduced in films 200-400 nm thick, and supporting the validity of the Dimitriadis model for measuring Young's modulus. The bulk and thin films, although cast from different solvents, are both crosslinked in the dry state, and are thus expected to have similar structures and elastic moduli. For films of lower pN$_3$Phe content, AFM yields moduli slightly higher than those obtained from tensile measurements (Table A.3).

Engineering of the elastic moduli of thin protein films by controlling pN$_3$Phe content should prove useful in cell culture experiments designed to study mechanosensitive cell behavior. An especially attractive prospect is the use of microfluidic mixing[15,39] to prepare protein substrates characterized by controlled gradients in elastic modulus.

Modulus control by variable irradiation. Elastic modulus gradients can also be prepared by variation in the radiation dose used for photocrosslinking. To demonstrate, we prepared a step-gradient by irradiating adjacent portions of an aE-66%-pN$_3$Phe film for increasing lengths of time. The elastic moduli measured (by AFM) at different locations on the film are shown in Figure A.10; the modulus increases slightly more than two-fold as the irradiation time increases from 20 to 300 sec. The majority of the rise in elastic modulus occurs over the first minute of exposure, consistent with the photolysis behavior reported previously.[24]

When the gradient film was washed to remove soluble protein, the thicknesses of the 20 sec and 30 sec zones were ca. 35% and ca. 20%, respectively, less than the thickness of the zones irradiated for longer periods, indicating incomplete crosslinking. Taking into account the known film height (as in the Dimitriadis calculation of the modulus) is essential for these gradient films, since variable film height would make the Hertz model inaccurate even as a comparative measure of the local elastic modulus.

Films that exhibit spatial variation in modulus on millimeter length scales offer unique advantages as substrates for the study of cell behavior. Large numbers of cells can be cultured on each zone

of a step-gradient substrate, allowing average cell properties to be measured as a function of elastic modulus on a single substrate. This approach minimizes reagent use and substrate preparation, and avoids lot-to-lot variation in the behavior of cultured cells. Observation of cell behavior at interfaces between stiff and soft materials has also proven instructive.[6] Films with more complex patterns of mechanical properties can also be envisioned. Irradiation through a mask, used previously to pattern proteins on solid supports,[24] could be easily adapted to the preparation of films with micropatterned moduli. Cell behavior on micropatterned materials has been the subject of a recent study.[40]

While step gradients are easy to characterize with a limited number of indentations, films with smooth gradients of elastic modulus could also be made via the variable irradiation approach by moving an opaque shutter continuously across the film.[41] Gradients could be implemented over a variety of length scales. The spatial resolution of the modulus measurement is limited only by the 300 nm radius of the tip used for indentation, and is adequate for measurement of the variation in mechanical properties under a single spread cell. Even higher resolution might be achieved through use of conventional sharp (< 20 nm) conical or pyramidal tips together with finite element analysis of the indentation process. Gradients extending over distances greater than the ca. 100 μm lateral piezo range of conventional AFM instruments could be characterized by using translational reference points in the sample.

Conclusions

Incorporation of the photosensitive amino acid *p*-azidophenylalanine into artificial proteins enables the photochemical synthesis of thin protein films of controlled elastic modulus. A film height-dependent indentation model, validated by bulk tensile measurements and finite element simulation, allows the elastic modulus to be determined with confidence by nanoindentation. The thin films prepared in this work enable new approaches to the study of mechanosensitive cell behavior in the context of coincident biological signals.

Acknowledgment

We gratefully acknowledge support of this research by the Center for the Science and Engineering of Materials at Caltech (NSF DMR-0520565) and by NIH grant EB1971. We thank Marissa Mock for NMR characterization and Doron Shilo for help with AFM measurements.

References and Notes

(1) Discher, D. E.; Janmey, P.; Wang, Y. L. *Science* **2005**, *310*, 1139-1143.

(2) Pelham, R. J.; Wang, Y. L. *Proc. Natl. Acad. Sci. U.S.A.* **1997**, *94* 13661-13665.

(3) Cukierman, E.; Pankov, R.; Stevens, D. R.; Yamada, K. M. *Science* **2001**, *294*, 1708-1712.

(4) Engler, A.; Bacakova, L.; Newman, C.; Hategan, A.; Griffin, M.; Discher, D. *Biophys. J.* **2004**, *86*, 617-628.

(5) Engler, A. J.; Richert, L.; Wong, J. Y.; Picart, C.; Discher, D. E. *Surf. Sci.* **2004**, *570*, 142-154.

(6) Lo, C. M.; Wang, H. B.; Dembo, M.; Wang, Y. L. *Biophys. J.* **2000**, *79*, 144-152.

(7) Gray, D. S.; Tien, J.; Chen, C. S. J. *Biomed. Mater. Res. A* **2003**, *66A*, 605-614.

(8) Wang, H. B.; Dembo, M.; Wang, Y. L. *Am. J. Physiol. - Cell Ph.* **2000**, *279*, C1345-C1350.

(9) Engler, A. J.; Griffin, M. A.; Sen, S.; Bonnetnann, C. G.; Sweeney, H. L.; Discher, D. E. *J. Cell Biol.* **2004**, *166*, 877-887.

(10) Engler, A. J.; Sen, S.; Sweeney, H. L.; Discher, *D. E. Cell* **2006**, *126*, 645-647.

(11) Engler, A. J.; Rehfeldt, F.; Sen, S.; Discher, D. E. *Methods Cell Biol.* **2007**, *83*, 521-545.

(12) Wang, Y. L.; Pelham, R. J. *In Molecular Motors and the Cytoskeleton*, Pt B, **1998**, *298*, 489-496.

(13) Maskarinec, S. A.; Tirrell, D. A. *Curr. Opin. Biotechnol.* **2005**, *16*, 422-426.

(14) Wong, J. Y.; Velasco, A.; Rajagopalan, P.; Pham, Q. *Langmuir **2003***, *19*, 1908-1913.

(15) Zaari, N.; Rajagopalan, P.; Kim, S. K.; Engler, A. J.; Wong, J. Y. *Adv. Mater.* **2004**, *16*, 2133-2137.

(16) Panitch, A.; Yamaoka, T.; Fournier, M. J.; Mason, T. L.; Tirrell, D. A. *Macromolecules* **1999**, *32*, 1701-1703.

(17) Welsh, E. R.; Tirrell, D. A. *Biomacromolecules* **2000**, *1*, 23-30.

(18) Di Zio, K.; Tirrell, D. A. *Macromolecules* **2003**, *36*, 1553-1558.

(19) Liu, J. C.; Heilshorn, S. C.; Tirrell, D. A. *Biomacromolecules* **2004**, *5*, 497-504.

(20) Mould, A. P.; Komoriya, A.; Yamada, K. M.; Humphries, M. J. *J. Biol. Chem.* **1991**, *266*, 3579-3585.

(21) Urry, D. W. *J. Phys. Chem. B* **1997**, *101*, 11007-11028.

(22) Kast, P.; Hennecke, H. *J. Mol. Biol.* **1991**, *222*, 99-124.

(23) Kirshenbaum, K.; Carrico, I. S.; Tirrell, D. A. *Chembiochem* **2002**, *3*, 235-237.

(24) Carrico, I. S.; Maskarinec, S. A.; Heilshorn, S. C.; Mock, M. L.; Liu, J. C.; Nowatzki, P. J.; Franck, C.; Ravichandran, G.; Tirrell, D.A. *J. Am. Chem. Soc.* **2007**, *129*, 4874-4875.

(25) Vinckier, A.; Semenza, G. *FEBS Lett.* **1998**, *430*, 12-16.

(26) Cappella, B.; Dietler, G. *Surface Science Reports* **1999**, *34*, 1-103.

(27) Heinz, W. F.; Hoh, J. H. *Trends Biotechnol.* **1999**, *17*, 143-150.

(28) Mahaffy, R. E.; Shih, C. K.; MacKintosh, F. C.; Kas, *J. Phys. Rev. Lett.* **2000**, *85*, 880-883.

(29) Richert, L.; Engler, A. J.; Discher, D. E.; Picart, C. *Biomacromolecules* **2004**, *5*, 1908-1916.

(30) Costa, K. D.; Yin, F. C. P. *J. Biomech. Eng.* **1999**, *121*, 462-471.

(31) Dimitriadis, E. K.; Horkay, F.; Maresca, J.; Kachar, B.; Chadwick, R. S. *Biophys. J.* **2002**, *82*, 2798-2810.

(32) Domke, J.; Radmacher, M. *Langmuir* **1998**, *14*, 3320-3325.

(33) Akhremitchev, B. B.; Walker, G. C. *Langmuir* **1999**, *15*, 5630-5634.

(34) Sharma, N. Ph.D. Thesis, University of Massachusetts Amherst, 2001.

(35) Nowatzki, P. J.; Tirrell, D. A. *Biomaterials* **2004**, *25*, 1261-1267.

(36) Yeoh, O. H. *Rubber Chem. Technol.* **1993**,*66*, 754-771.

(37) Flory, P. J. *Principles of Polymer Chemistry*; Cornell University Press: Ithaca, NY, 1953.

(38) Lillie, M. A.; Gosline, J. M. *Biopolymers* **2002**, *64*, 115-126.

(39) Jeon, N. L.; Dertinger, S. K. W.; Chiu, D. T.; Choi, I. S.; Stroock, A. D.; Whitesides, G.M. *Langmuir* **2000**, *16*, 8311-8316.

(40) Stevens, M. M.; George, J. H. *Science* **2005**, *310*, 1135-1138.

(41) Pucci, V.; Raggi, M. A.; Svec, F.; Frechet, J. M. J. *J. Sep. Sci.* **2004**, *27*, 779-788.